Synthetic Metals 259 (2020) 116259

Contents lists available at ScienceDirect

Synthetic Metals

journal homepage: www.elsevier.com/locate/synmet

Competing charge trapping and percolation in core-shell single wall carbon nanotubes/ polyaniline nanostructured composites

Rakibul Islam[a,*], Anthony N. Papathanassiou[b], Roch Chan-Yu-King[c], Carole Gors[a], Frédérick Roussel[a,1]

[a] Univ. Lille, CNRS, INRA, ENSCL, UMR 8207, UMET, Unité Matériaux et Transformations, F 59 000 Lille, France
[b] National and Kapodistrian University of Athens, Physics Department, Solid State Physics Section, Panepistimiopolis, GR15784 Zogarfos, Athens, Greece
[c] University of Science and Arts of Oklahoma, Chickasha, OK 73018, USA

ARTICLE INFO

Keywords:
Polymer composites
Interfacial capacitance
Electrical percolation

ABSTRACT

Core-shell single wall carbon nanotube (SWCNT)/ polyaniline (PANI) nanocomposites were chemically synthesized and their structural, morphological, and dielectric properties were investigated as a function of the nanofiller content. X-ray diffraction (XRD), field emission scanning electron microscopy (FE-SEM) and transmission electron microscopy (TEM) images confirm the core-shell nanostructural features of the composites. Broadband dielectric spectroscopy allows the detection of an interfacial dielectric relaxation mechanism which is quite dependent on the dispersion of nanoparticles into the semi-conducting polyaniline matrix. Furthermore, the relaxation process analysed through Kohlrausch-William-Watts (KWW) model, is found to take place at lower nanofiller loading but progressively fades away on increasing the amount of SWCNT, yielding relaxation spectra which gradually resemble that of a pure conductor. In addition, it is found that competing processes between electrical percolation and interfacial capacitance effects are inherently dependent on the carbon-filler content. Such a behaviour is ascribed to charge trapping and de-trapping phenomena occurring at core-shell interfaces. The possibility of tuning the composition of the nanocomposites in order to trigger an interplay between capacitance and dc-electrical conduction can be envisioned for their application in the next generation of organic-based supercapacitor or gate memory devices.

1. Introduction

The past decade has witnessed the development of binary nanocomposites derived from combining carbonaceous nanofillers dispersed in various polymer matrices. Owing to their interesting electrical, thermal and mechanical properties [1–3], these materials have attracted enormous attention because of their potential widespread commercial applications or use in specialized advanced technology. For example, it has been recently reported that the incorporation of graphene nanofillers in polymers enhances the performance of piezo-resistive sensors [4] and multilayer graphenes/polymer composites can function as highly efficient thermal interface materials [2]. More recent research with the use of carbon nanotubes/polyaniline(PANI) reveals that the composite materials can be used, e.g., as robust flexible electronic gas sensors [5], a chemosensors [6], or pseudocapacitive materials with high cycling stability [7]. In recent development on improved energy conversion and energy storage of prototypical devices, it has been found that a) SWCNT/polymer fillers can be used as charge storage elements when incorporated in the floating gate of a metal-insulator semiconductor [8] b) PANI nanowire arrays grafted on reduced graphene oxide exhibits enhanced electrochemical behaviour and are promising nanocomposites for use in high performance supercapacitors [9] c) self-aligned reduced graphene oxide/epoxy nanocomposites are capable of high charge accumulation at the filler/matrix interface and they present excellent electromagnetic shielding properties [10] d) CNTs and graphene composites demonstrate good conductivity and high volumetric energy density [11] and e) battery electrodes, derived from combining diverse porous carbons with structurally designed PANI, present superior power density as compared to their Li-ion counterparts [12].

In general, the characteristics of the nanocomposite materials are greatly dependent on their methods of preparation/protocols of synthesis and the dimension (O, 1 or 2D) of the nano-carbonaceous filler which affects the kinetics of crystallization process of the polymer

* Corresponding author.
E-mail addresses: rakibul.islam@univ-rouen.fr, rakibulphysics@gmail.com (R. Islam).
[1] In memoriam to our beloved colleague Frédérick Roussel.

https://doi.org/10.1016/j.synthmet.2019.116259
Received 11 July 2019; Received in revised form 8 November 2019; Accepted 29 November 2019
Available online 09 December 2019
0379-6779/ © 2019 Elsevier B.V. All rights reserved.

[13]. The properties (e.g. mechanical, thermal and electrical [13,14]) of the resulting materials and their performance are controlled through crucial parameters such as, the amount and quality of the filler dispersion, the morphology of their interfacial spacing, and the conducting filler/host interactions etc. For example, it has been shown that a) definite amounts of reduced graphene oxide (RGO) in PANI [15] or CNTs in PMMA [16] can play a synergistic role in effecting 2D or 3D electrical and thermal percolations in the nanocomposites, b) complex micro/nano interfacial effects are instrumental in controlling the charge and phonon transport mechanisms in composites like RGO/PANI [17] or in graphene multi-layered graphene composites [2]. In addition, the effect of effective interfacial resistance on thermal conductivity in hybrid system has recently been reported [18]. While methods of improvement of electrical conductivity in CNTs/PANI have been reviewed [19–22] and there are numerous reports describing the capacitance effect in these composites [12,23,24], nevertheless, we believe that further research related to the competing nature of the electrical vs. interfacial capacitance effect is warranted.

More specifically, in this work, we discuss a competition between interfacial capacitance and electrical percolation in core-shell SWCNT/PANI composites. It has been reported that the fabrication of the above composites can be achieved via different methods such as electrochemical polymerization, template polymerization, enzymatic polymerization, photo-polymerization, plasma polymerization, or chemical polymerization [23]. Since in situ chemical polymerization process for the preparation of SWCNT/PANI are known to provide fairly homogeneous polymer composites because growing PANI chains in solution can easily combined with fillers to form hybrids resulting in further improved functional properties [23,25]. We have adopted and modified this method by carrying it under sonication in hope to disentangle to some extent and better disperse the SWCNT during polymerization.

Field Emission Scanning Electron Microscopy (FE-SEM) and Transmission Electron Microscopy (TEM) were employed to confirm the composite core-shell structures. Complex dielectric permittivity spectra obtained from Broadband dielectric spectroscopy (BDS) are analyzed within the framework of the Kohlrausch-Williams-Watts (KWW) model. The relaxation process and dc-electrical conductivity are evaluated as a function of the SWCNT loading. The relationship between charge capacitance and percolation behavior of dc-electrical conductivity is investigated according to charge trapping and de-trapping processes taking at core-shell SWCNT/PANI interfaces.

2. Materials and methods

Most chemicals used were obtained from Aldrich Chemical except the single-walled carbon nanotube (> 90 % purity; containing 3.96 % OH) which were purchased from Times Nano (China). SWCNT/PANI nanocomposites were synthesized through an in situ chemical polymerization method combining aniline monomers, SWCNT, ammonium peroxydisulfate (APS) (oxidizing agent) and 1.0 M (aq.) HCl as dopant. Nanocomposites with various weight fractions of SWCNT, (ranging from 0.034 vol-% (0.01 wt-%) to 12.25 vol-% (17 wt-%)) were prepared. A typical procedure is as follows for the synthesis of pure PANI and a PANI composite with 0.068 vol-% SWCNT:

A.) Synthesis of Pure PANI

Into a 30-ml beaker containing a magnetic stir bar was placed a solution of 0.347 g (3.726 mmol) aniline in 18.0 ml of 1.0 M HCl (aq). This mixture was magnetically stirred for 1 h at room temperature. To this vigorously stirred solution was then added (dropwise, via pipet) a solution of 0.913 g (4.001 mmol) APS in 7.0 ml of 1.0 M HCl (aq). Magnetic stirring of the resulting solution was continued for another 24 h at room temperature. The deep green solid product was then suction filtered, and then washed sequentially with copious amounts of de-ionized water (to rid of the excess HCl (aq), anilinium monomers and residual APS), acetone (to remove aniline oligomers and organic by-products) until a colourless filtrate was obtained. The composites were further rinsed with hexanes to remove the residual acetone after which it was dried (50.0 °C; 12 h) under high vacuum and then stored in a desiccator containing $CaCl_2$ as drying agent.

A.) Synthesis of SWCNT/PANI composites

Into a glass test tube was sequentially added 3.50 mg (0.292 mmol) SWCNT, 0.347 g (3.726 mmol) aniline and 18.0 ml of 1.0 M HCl (aq.) The tube was then placed into a sonicator (Branson ultrasonic cleaner, model CPX 3800 H-E; 5.7 litter tank) and the mixture was sonicated for 1 h at room temperature. It was then transferred into a beaker, and a solution of 0.913 g (4.001 mmol) APS in 7.0 ml of 1.0 M HCl (aq.) was added. The resulting mixture was magnetically stirred for 24 h at room temperature. The composites formed was suction filtered and then sequentially washed with de-ionized water, acetone (until a colourless filtrate was obtained) and further rinsed with hexanes. They were then high vacuum dried and stored as describes above.

Pellets of the as-prepared Pure PANI and nanocomposites were prepared from pulverized powder with the use of a hydraulic press (450 MPa) which provided test samples having a diameter of 13 mm and a thickness of 270 ± 20 μm.

X-ray diffraction (XRD) measurements were carried out via a curved multidetector INEL-CPS 120 set up. Lindeman glass capillary tubes (diameter 0.70 mm) was used to place the samples and irradiated with a collimated monochromic beam (λ = 0.154056 nm). Samples were rotated around the vertical axis of the goniometer head. FE-SEM (Hitachi S4700 operating at 6 kV) and TEM (FEI Technai G2 operating at 20 kV) were employed to investigate the morphological and structural characteristics of SWCNT/PANI composites. The pellets were then placed between aluminium electrodes and dielectric permittivity measurements were carried out at room temperature on a Modulab-MTS test system (Solartron Analytical-Amtek) in the frequency (ƒ) range of 1Hz-1 MHz with an amplitude of the oscillating voltage set at 100 mV. The dielectric spectra were fitted with the Grafity software [26].

3. Results and discussion

Fig. 1 depicts XRD spectra of pure PANI, pure SWCNT and SWCNT/PANI composites. As shown in Fig. 1, XRD pattern of pure SWCNT exhibits characteristic diffraction peaks at 2θ ~ 26.2° and ~42.8°, which are correspond to (002) and (100) crystal plane [27–29]. Pure PANI XRD analysis exhibits that a broad peak is observed from 2θ ~ 10° to 2θ ~ 30° indicating amorphous PANI along with a sharper peak at 2θ ~ 25° which is assigned to the (110) reflection of crystallographic plane of the orthorhombic structure reported for semi-crystalline PANI [15,30]. For SWCNT/PANI composites, the peak (2θ ~ 26.2°) of SWCNT and the peak of PANI (2θ ~ 25°) are overlapped and the peak is shifted towards higher 2θ. The result is in good agreement with the previous result of PANI/SWCNT composites reported by N. G. Gull et al. [20]. In case of SWCNT/PANI composites with 12.25 vol-% SWCNT content, the peak is appeared at 2θ ~42.8° which confirm the presence of SWCNT into the composites.

Fig. 2a displays the morphology of chemically synthesized pure PANI which exhibits interconnected nanofibers with an average diameter of ca. 79 ± 15 nm. The SEM images of SWCNT/PANI nanocomposites filled with different concentrations of SWCNT are shown in Fig. 2b–d. Fig. 2b displays a mixed morphology containing SWCNT with domains rich in PANI nanofibers having a diameter of ca. 60 ± 10 nm. Fig. 2c reveals a nice encapsulation of SWCNT by PANI forming core (SWCNT)-shell (PANI) structures. This feature is further confirmed via TEM analysis as illustrated in Fig. 2d for a sample containing 12.25 vol-% SWCNT (50 nm scale bar). The diameter of the core-shell nanostructures is ca. 75 ± 15 nm with PANI nanofiber shells (having diameters of ca. 25 − 35 nm) deposited around the SWCNTs. It is believed

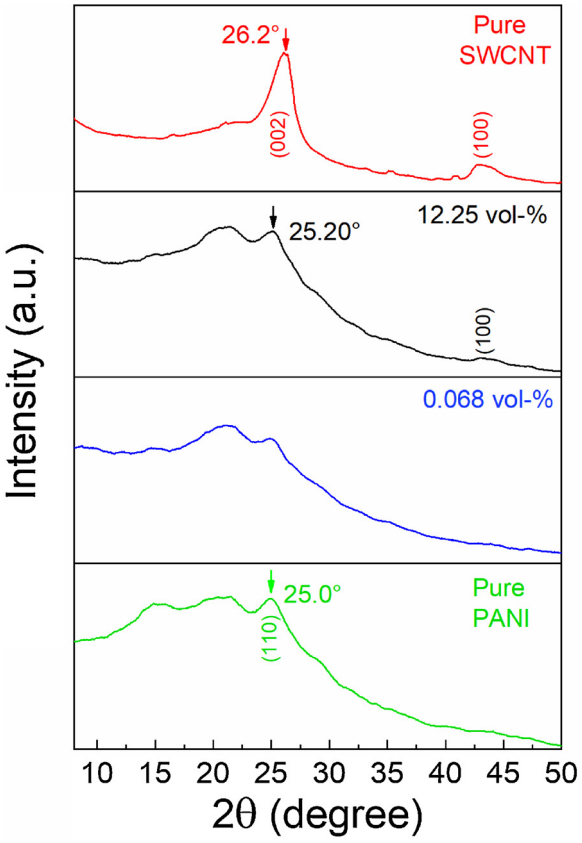

Fig. 1. XRD pattern of pure PANI, pure SWCNT, and SWCNT/PANI composites.

that the mechanism of the encapsulation process involves a preliminary stretching step of the molecular chain of PANI followed by its pairing with the SWCNT and wrapping of the latter with the polymer host until an equilibrium is achieved [31]. Such a core-shell feature is favoured by good aromatic basal ring π-π interactions between PANI and SWCNT

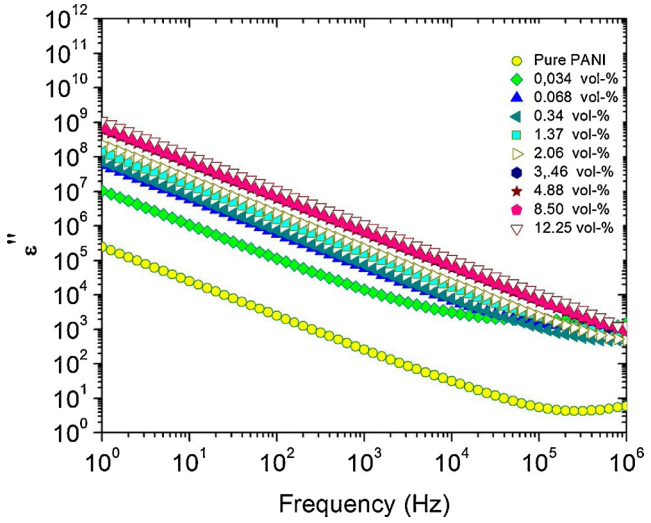

Fig. 3. Imaginary part (ε") of the complex dielectric permittivity vs frequency for pure PANI, and SWCNT/PANI composites containing 0.034, 0.068, 0.34, 1.37, 2.06, 3.46, 4.88, 8.50, and 12.25 vol-% SWCNT, respectively.

[32–34]. In this process, the aromatic rings of PANI are envisioned to gradually orient such that their planes are parallel to those of SWCNT, thereby favouring good intermolecular interactions. It is also observed that with increasing SWCNT loading the diameter of core-shell composites is reduced from ca. 180 ± 30 nm (for 2.06 vol-% SWCNT) to ca. 75 ± 15 nm (for a sample with 12.25 vol-% SWCNT) i.e., the diameter of PANI nanofibers is reduced with increasing inclusion of fillers into matrix.

The imaginary part (ε′′) of the complex permittivity vs frequency recorded at room temperature for PANI and SWCNT/PANI composites of various compositions is depicted in Fig. 3. The imaginary part of the complex permittivity $\varepsilon^* = \varepsilon' + j\varepsilon''$ is related to the real part of the complex electrical conductivity $\sigma^* = \sigma' + j\sigma''$ through the following relation [35]:

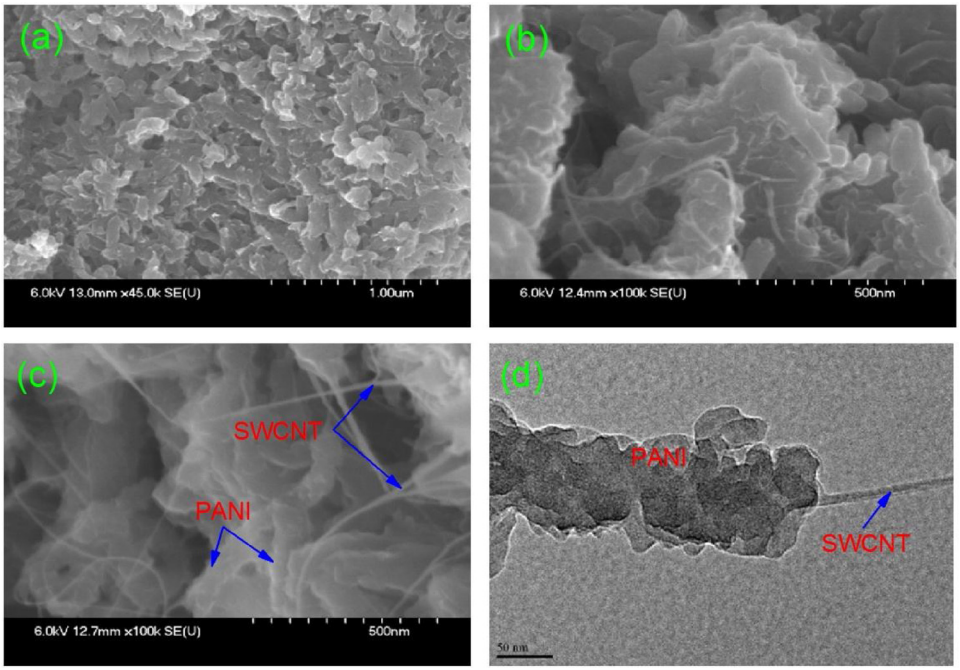

Fig. 2. Images observed by FE-SEM for (a) pure PANI, and SWCNT/PANI nano-composites with (b) 2.06 vol-% and (c) 8.50 vol-% SWCNT respectively and (d) HR-TEM image for SWCNT/PANI nano-composites with 12.25 vol-% SWCNT.

$$\sigma' = 2\pi f \varepsilon_0 \varepsilon'' \quad (1)$$

where f denotes the frequency of the externally applied harmonic voltage and ε_0 is the permittivity of free space. We observe that $\varepsilon''(f)$ values increase with increasing SWCNT loading, which is related with the subsequent increase of the dc conductivity. Also, the gradual increase of the amount of SWCNT resulted in a relaxation process which appears in the range of 10^3-10^5 Hz. Thus, the relaxation mechanism which is absent in the behaviour of the pristine PANI, is attributed to the presence of SWCNT. In the MHz region, the low-frequency tail of an additional relaxation mechanism is observed, with its maximum located beyond the upper detection limit of our impedance analyzer; we ascribe it to a transmission line effect and its study is beyond the scope of the present work.

To gain further insights into the spectrum of imaginary part (ε'') of complex permittivity, the experimental data were analyzed via the following a function:

$$\varepsilon''(f) = \varepsilon_1''(f) + \varepsilon_2''(f) \quad (2)$$

Eq. (2) deals with the low-frequency region of the spectrum where the ac conductivity is frequency independent and is equal to the dc-conductivity (σ_{dc}) which is defined as:

$$\varepsilon_1''(f) = \sigma_{dc}/\varepsilon_0(2\pi f)^n \quad (3)$$

where n is a fractional exponent close to 1. Furthermore, in the high-frequency dispersive region a dielectric loss is observed; this phenomenon is interpreted via the Fourier transform of the Kohlrausch-Williams-Watts (KWW) stretched exponential functions given by the equation [36]:

$$\varepsilon_2''(t) = \Delta\varepsilon_{KWW} e^{-\left(\frac{t}{\tau_{kww}}\right)^{\beta}} \quad (4)$$

where $\Delta\varepsilon_{KWW}$ is the relaxation strength, τ_{KWW} is the KWW-relaxation time, and β is the stretching exponent ($0 < \beta \leq 1$) which reaches unity for ideal Debye systems. We wish to point out that the KWW function is usually employed in the literature to fit dielectric loss peaks in conducting polymers and composites [37,38]. Because this function has allowed us to analyse and successfully interpret dielectric and electrical phenomena in composites made of PANI/graphene oxide, we have decided to use it in this study [17,39]. We are particularly interested in determining the relationship between % SWCNT content and capacitance effects (expressed through $\Delta\varepsilon_{KWW}$) upon SWCNT, rather than the shape parametrs of the fitting function.

Fig. 4a–d show the frequency dependence of ε'' experimental data (symbols) and fitting curves (solid and dashed lines) for pure PANI and SWCNT/PANI nanocomposites. For pure PANI, all data points (apart from the high frequency transmission line effect) lie on a straight line with a slope of -1 which is attributed to the dc conductivity term. The experimental data of nanocomposites are described by the dc conductivity and KWW relaxation overlap. Dispersing SWCNT around the PANI host enriches the nanocomposites in host-guest interfaces, which induces an electrical inhomogeneity in the nanocomposites. Consequently, an interfacial polarization occurs which produces a relaxation peak. On increasing the SWCNT loading, spacing between the semi conducting PANI and SWCNT is reduced, thereby the density of interfaces is increased. This change favours an enhancement in charge trapping and as a result, the intensity of the relaxation peak decreases upon raising the SWCNT fraction (Fig. 5a), while σ_{dc} increases (Fig. 5c). In addition, it can be seen that the relaxation peak maximum f_{max} retrieved from the KWW function are increased with SWCNT fraction rises (Fig. 5b). Therefore, the topology and conduction efficiency of the percolation network of the composites is optimized on increasing SWCNT loading and an increase of the dc conductivity is subsequently observed.

The relaxation mechanism observed in the nanocomposites is lacking in neat PANI. Its presence is therefore correlated with the heterogeneous structure of the composites. Moreover, the relaxation dynamics depends on SWCNT content: in Fig. 5b, the relaxation peak maximum f_{max} shifts towards higher frequencies vs the volume fraction of SWCNT. To a first approximation, the nanocomposites can be simulated as if they are made of a two phase system. Indexes 1 and 2 indicate the host PANI and dispersed SWCNT phases, respectively. Sillars [40] considered the case of dispersed spheroid inclusions of axes a and b, respectively and calculated the relaxation time $\tau = 1/fmax$ in terms of the dc conductivity $\sigma_{dc,i}$ and (relative) dielectric constant ε_i (where i = 1, 2), as well as the volume fraction υ_2 of the dispersed phase:

$$\tau = \varepsilon_0 \frac{\varepsilon_1 + A_0(1-v)(\varepsilon_2 - \varepsilon_1)}{\sigma_{dc,1} + A_0(1-v_2)(\sigma_{dc,2} - \sigma_{dc,1})} \quad (5)$$

Where A_0 is a shape parameter factor, which is a positive number less than unity. If SWCNT are considered approximately as oblate spheroids with a > > b, A0 = [ln(2a/b)-1](b/a)^2 [40] PANI, the host phase 1, is a good semiconductor, while SWCNT, phase 2, is highly conductive, i.e., $\sigma_{dc,2} > > \sigma_{dc,\ 1}$ and $\varepsilon_1 > > \varepsilon_2$. Subsequently, for prolate conducting spheroid inclusions, (given that $\tau = 1/fmax$), eq. (A1) can be written:

$$\tau \cong \varepsilon_0 \frac{\varepsilon_1[1 - A_0(1-v_2)}{\sigma_{dc,2} A_0(1-v_2)} \quad (6)$$

Differentiating Eq. (6) with respect to the SWCNT volume fraction υ_2, we get:

$$\frac{dlnf_{max}}{dv_2} \approx \frac{(1-v_2)^2 - A_0(1-v_2) + 1}{(1-v_2)v_2} \quad (7)$$

Since $1 > \upsilon_2 > 0$ and $(1\text{-}\upsilon_2)^2\text{-}A_0(1\text{-}\upsilon_2)+1 > 0$ (provided that $1 > \upsilon_2 > 0$), we get $d\ln f_{max}/d\upsilon_2 > 0$. Fig. 5b indicates that log f_{max} shifts towards higher frequencies on increasing volume fraction υ2. This finding is indeed, in accord with the above mentioned predictions of the Sillars model for elongated prolate conducting spheroids dispersed into a semiconducting matrix.

The dc conductivity values obtained by fitting Eq. (2) to the data points of Fig. 3, are plotted against the volume fraction (φ) of SWCNT content. The result is depicted in Fig. 5c. It has been described that percolation theory for systems consisting of conducting inclusions dispersed into an insulating matrix requires a critical volume fraction φ_C needed for the transition from an insulator state to a conducting one. Accordingly, the dc conductivity at constant temperature is given by the equation:

$$\sigma_{dc}(\varphi)(\varphi - \varphi_C)^r \quad (8)$$

where r is a (model-dependent) universal constant, ranging roughly from 1 to 2 (i.e, r is 2 and 1.3 for 3D and 2D systems, respectively) [41,42]. The fitting Eq. (8) with $\varphi_c = 0.004 \pm 0.002$ and $r = 1.0 \pm 0.1$ indeed indicates the occurrence of a percolation network. Above φ_c, with higher φ_c, a transition from the semi-insulating to a conducting state takes place.

It is known that the electric charge transport within a homogeneously disordered solid, where disorder is space-invariant (i.e., a carrier senses the same degree of disorder of the surrounding environment), is capable to induced charge localization, depending on the frequency of the external electric field. This phenomenon eventually is accompanied by the appearance of a dielectric loss peak. In this case, σ_{dc} is correlated to f_{max} and $\Delta\varepsilon$, according to the Barton - Nakajima – Namikawa (BNN) [43]: $\sigma_{dc} = 2\pi p \varepsilon_0 \Delta\varepsilon f_{max}$, where p is an empirical parameter and is roughly equal to 1.7 [44]. Fig. 5b depicts an evaluation of f_{max} as a function of SWCNT content. However, the results indicate that the BNN relation cannot be applied in our case, indicating that the relaxation peak does not stem from the motion of free carriers in a homogeneously disordered matrix rather, a relaxation may occur due to charge trapping at the interfaces of PANI and SWCNT. According to the latter scenario, percolation competes with interfacial charge trapping, as evidenced by the reduction of $\Delta\varepsilon$ (which is a measure of the

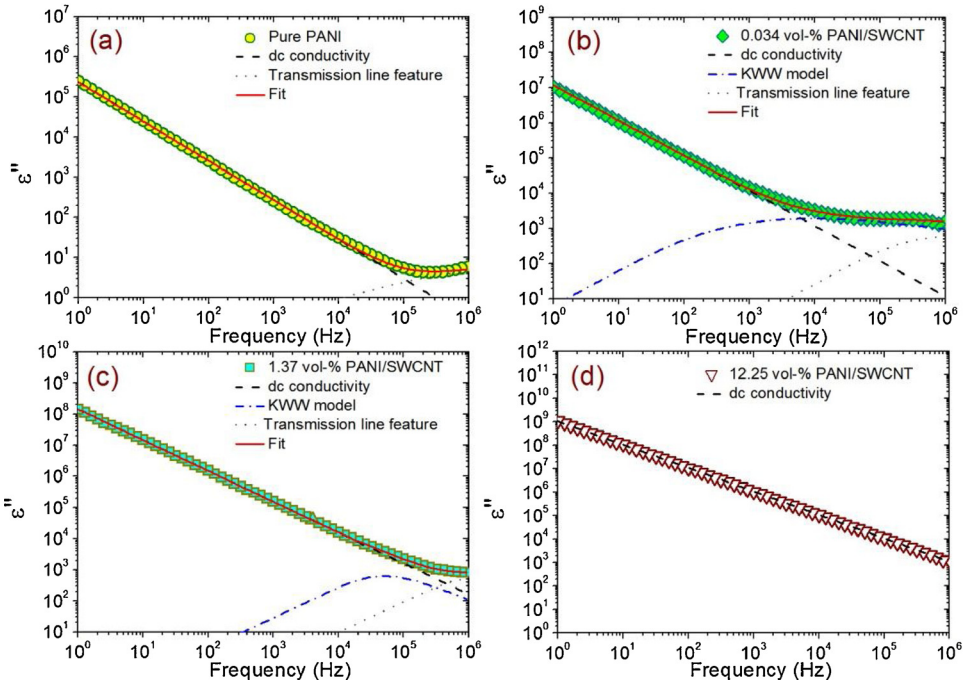

Fig. 4. Imaginary part ε″ of the complex dielectric permittivity vs frequency for (a) pure PANI, (b) 0.034 vol-% SWCNT/PANI, (c) 1.37 vol-% SWCNT/PANI, and (d) 12.25 vol-% SWCNT/PANI. Symbols are experimental data point, whereas red lines are the best fitting curves of a conductivity line (black color) with slope -1, KWW peak (blue colour). (For interpretation of the references to colour in this figure legend, the reader is referred to the web version of this article).

density of trapped charge) upon raising the φ value [45]. As seen in Fig. 5d, where $\log\sigma_{dc}$ is plotted vs $\log\Delta\varepsilon$ for all nanocomposites, a systematic enhancement of macroscopic dc conductivity takes place at the expense of charge trapping which is speculated to be caused by the structural and electrical heterogeneity of the composites. Further analysis by FTIR, RAMAN, XRD is required to alternatively support the electrical results. For example, in comparison to pure PANI, the XRD pattern of hybrid SWCNT/PANI nanocomposites (shown in Fig. 1) detect noticeable differences in the sharpness of the peaks, which is correlated to the crystallinity of nanocomposites. The effective electrical properties of the nanocomposites can be correlated to the changing behaviour of the crystallinity in the nanocomposites.

4. Conclusions

In conclusion, chemically synthesized core-shell single wall carbon nanotubes/ polyaniline nano-composites were synthesized and characterized in relation to the carbonaceous nano-filler content. XRD, FE-SEM and TEM images confirm the core-shell nano-structured features of the SWCNT/PANI composites. Frequency-domain dielectric studies reveal an interfacial dielectric relaxation mechanism associated with the presence and amount of the dispersed nano-particles in the semi-conducting polyaniline matrix. Depending on the filler content, percolation competes with interfacial capacitance effects. The electric charge percolation critical volume fraction obtained by fitting eq. (8) to the data points depicted in Fig. 5c, is $\varphi_c = 0.4$ %. Above this critical fraction, the intensity $\Delta\varepsilon_{KWW}$ of relaxing trapped carriers drops significantly. Therefore, a φ_c of 0.4 % is the optimal fraction of SWCNT needed to

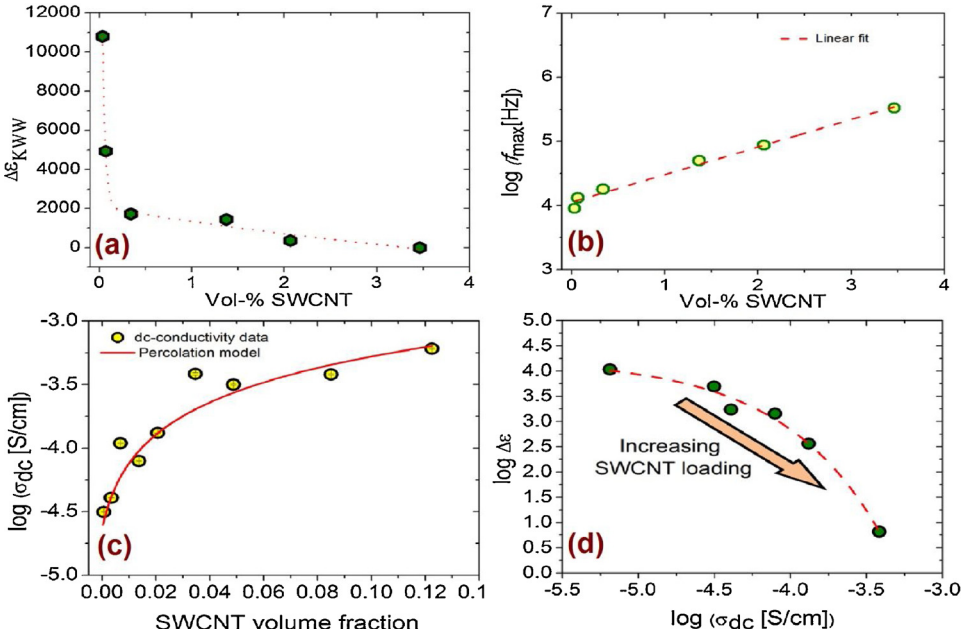

Fig. 5. Dependence of the fitting parameters of the KWW model on SWCNT loading: (a): peak intensity and (b): the logarithm of the peak maximum f_{max}, (c) dc conductivity vs vol-% SWCNT (symbols are experimental data point, whereas red line is the best fit of the percolation model) and (d) competition of $\log\sigma_{dc}$ against $\log\Delta\varepsilon$ (the SWCNT content balances dc conductivity versus capacitance effects).

produce highly conductive composites, with minimal SWCNT loading. We ascribed our results to a charge trapping and de-trapping phenomenon, which is believed to take place at core-shell interface of the nanocomposites. By tuning the SWCNT composition, a balance between capacitance and dc-electrical conduction is possible and the results could be applied in the fabrication of promising materials of tunable conductivity and charge storage capability, which can be used in energy storage and gate memory devices.

Declaration of Competing Interest

We acknowledge that there is no conflict of interest in this work.

Acknowledgements

Anthony N. Papathanassiou acknowledges the University of Lille 1 (Villeneuve d'Ascq, 59650, France) for inviting him as a Visiting Professor. Roch Chan-Yu-King is grateful for the financial support of University of Lille 1. He also thanks the University of Science and Arts of Oklahoma for its partial contribution (via the Gladys Anderson Emerson Fund) to this project. Dr. Ahmed Addad is kindly acknowledged for his help with TEM.

Appendix A. Supplementary data

Supplementary material related to this article can be found, in the online version, at doi:https://doi.org/10.1016/j.synthmet.2019.116259.

References

[1] Z. Spitalsky, D. Tasis, K. Papagelis, C. Galiotis, Carbon nanotube-polymer composites: chemistry, processing, mechanical and electrical properties, Prog. Polym. Sci. 35 (2010) 357–401, https://doi.org/10.1016/j.progpolymsci.2009.09.003.
[2] K.M.F. Shahil, A.A. Balandin, Graphene–multilayer graphene nanocomposites as highly efficient thermal interface materials, Nano Lett. 12 (2012) 861–867, https://doi.org/10.1021/nl203906r.
[3] J.N. Coleman, U. Khan, W.J. Blau, Y.K. Gun'ko, Small but strong: a review of the mechanical properties of carbon nanotube-polymer composites, Carbon N. Y. 44 (2006) 1624–1652, https://doi.org/10.1016/j.carbon.2006.02.038.
[4] P. Costa, J. Nunes-Pereira, J. Oliveira, J. Silva, J.A. Moreira, S.A.C. Carabineiro, J.G. Buijnsters, S. Lanceros-Mendez, High-performance graphene-based carbon nanofiller/polymer composites for piezoresistive sensor applications, Compos. Sci. Technol. 157 (2017) 241–252, https://doi.org/10.1016/j.compscitech.2017.11.001.
[5] L. Xue, W. Wang, Y. Guo, G. Liu, P. Wan, Flexible polyaniline/carbon nanotube nanocomposite film-based electronic gas sensors, Sens. Actuators B Chem. 244 (2017) 47–53, https://doi.org/10.1016/j.snb.2016.12.064.
[6] Y. Liao, C. Zhang, Y. Zhang, V. Strong, J. Tang, X.G. Li, K. Kalantar-Zadeh, E.M.V. Hoek, K.L. Wang, R.B. Kaner, Carbon nanotube/polyaniline composite nanofibers: facile synthesis and chemosensors, Nano Lett. 11 (2011) 954–959, https://doi.org/10.1021/nl103322b.
[7] D. Liu, X. Wang, J. Deng, C. Zhou, J. Guo, P. Liu, Crosslinked carbon nanotubes/polyaniline composites as a pseudocapacitive material with high cycling stability, Nanomaterials 5 (2015) 1034–1047, https://doi.org/10.3390/nano5021034.
[8] M. Alba-Martin, T. Firmager, J. Atherton, M.C. Rosamond, D. Ashall, A. Al Ghaferi, A. Ayesh, A.J. Gallant, M.F. Mabrook, M.C. Petty, D.A. Zeze, Improved memory behaviour of single-walled carbon nanotubes charge storage nodes, J. Phys. D Appl. Phys. 45 (2012) 295401http://stacks.iop.org/0022-3727/45/i=29/a=295401.
[9] L. Wang, Y. Ye, X. Lu, Z. Wen, Z. Li, H. Hou, Y. Song, Hierarchical nanocomposites of polyaniline nanowire arrays on reduced graphene oxide sheets for supercapacitors, Sci. Rep. 3 (2013) 3568, https://doi.org/10.1038/srep03568.
[10] N. Yousefi, X. Sun, X. Lin, X. Shen, J. Jia, B. Zhang, B. Tang, M. Chan, J.-K. Kim, Highly aligned graphene/polymer nanocomposites with excellent dielectric properties for high-performance electromagnetic interference shielding, Adv. Mater. 26 (2014) 5480–5487, https://doi.org/10.1002/adma.201305293.
[11] T. Kim, G. Jung, S. Yoo, K.S. Suh, R.S. Ruoff, Activated graphene-based carbons as supercapacitor electrodes with macro- and mesopores, ACS Nano 7 (2013) 6899–6905, https://doi.org/10.1021/nn402077v.
[12] X. Wang, D. Wu, X. Song, W. Du, X. Zhao, D. Zhang, Review on Carbon/Polyaniline hybrids: design and synthesis for supercapacitor, Molecules 24 (2019) 2263–2280, https://doi.org/10.3390/molecules24122263.
[13] J.-Z. Xu, G.-J. Zhong, B.S. Hsiao, Q. Fu, Z.-M. Li, Low-dimensional carbonaceous nanofiller induced polymer crystallization, Prog. Polym. Sci. 39 (2014) 555–593, https://doi.org/10.1016/j.progpolymsci.2013.06.005.
[14] M. Bhattacharya, Polymer nanocomposites—a comparison between carbon nanotubes, graphene, and clay as nanofillers, Materials (Basel) 9 (2016).
[15] R. Islam, R. Chan-Yu-King, J.-F. Brun, C. Gors, A. Addad, M. Depriester, A. Hadj-Sahraoui, F. Roussel, Transport and thermoelectric properties of polyaniline/reduced graphene oxide nanocomposites, Nanotechnology 25 (2014) 475705, , https://doi.org/10.1088/0957-4484/25/47/475705.
[16] P. Bonnet, D. Sireude, B. Garnier, O. Chauvet, Thermal properties and percolation in carbon nanotube-polymer composites, Appl. Phys. Lett. 91 (2007) 201910, , https://doi.org/10.1063/1.2813625.
[17] R. Islam, A.N. Papathanassiou, R.C.Y. King, J.-F. Brun, F. Roussel, Evidence of interfacial charge trapping mechanism in polyaniline/reduced graphene oxide nanocomposites, Appl. Phys. Lett. 107 (2015) 53102, https://doi.org/10.1063/1.4927591.
[18] D. Pratap, R. Islam, P. Al-Alam, J. Randrianalisoa, N. Trannoy, Effect of air confinement on thermal contact resistance in nanoscale heat transfer, J. Phys. D Appl. Phys. 51 (2018) 125301http://stacks.iop.org/0022-3727/51/i=12/a=125301.
[19] L.C. Mariano, R.V. Salvatierra, C.E. Cava, M. Koehler, A.J.G. Zarbin, L.S. Roman, Electrical properties of self-assembled films of polyaniline/carbon nanotubes composites, J. Phys. Chem. C 118 (2014), https://doi.org/10.1021/jp502650u 24811−2481.
[20] N. Gull, S.M. Khan, A. Islam, S. Zia, M. Shafiq, A. Sabir, M.A. Munawar, M.T.Z. Butt, T. Jamil, Effect of different oxidants on polyaniline/single walled carbon nanotubes composites synthesized via ultrasonically initiated in-situ chemical polymerization, Mater. Chem. Phys. (2016) 39–46, https://doi.org/10.1016/j.matchemphys.2015.12.048.
[21] S. Qu, Q. Yao, L. Wang, J. Hua, L. Chen, A novel hydrophilic pyridinium salt polymer/SWCNTs composite film for high thermoelectric performance, Polymer (Guildf) 136 (2018) 241–252, https://doi.org/10.1016/j.polymer.2017.12.048.
[22] N.I. Ibrahim, A.S. Wasfi, A comparative study of polyaniline/MWCNT with polyaniline/SWCNT nanocomposite films synthesized by microwave plasma polymerization, Synth. Met. 250 (2019) 49–53, https://doi.org/10.1016/j.synthmet.2019.02.007.
[23] B. Che, H. Li, D. Zhou, Y. Zhang, Z. Zeng, C. Zhao, C. He, E. Liu, X. Lu, Porous polyaniline/carbon nanotube composite electrode for supercapacitors with outstanding rate capability and cyclic stability, Compos. Part B Eng. 165 (2019) 675–678, https://doi.org/10.1016/j.compositesb.2019.02.026.
[24] P. Liu, J. Yan, Z. Guang, Y. Huang, X. Li, W. Huang, Recent advancements of polyaniline-based nanocomposites for supercapacitors, J. Power Sources 424 (2019) 108–130, https://doi.org/10.1016/j.jpowsour.2019.03.094.
[25] B. Philip, J. Xie, J.K. Abraham, V.K. Varadan, Polyaniline/carbon nanotube composites: starting with phenylamino functionalized carbon nanotubes, Polym. Bull. 53 (2005) 127–138, https://doi.org/10.1007/s00289-004-0321-x.
[26] Focus software is avaiable at http://www.cemhti.cnrs-orleans.fr/pot/software/focus.html, (n.d.).
[27] G. Liu, Y. Zhao, K. Deng, Z. Liu, W. Chu, J. Chen, Y. Yang, K. Zheng, H. Huang, W. Ma, L. Song, H. Yang, C. Gu, G. Rao, C. Wang, S. Xie, L. Sun, Highly dense and perfectly aligned single-walled carbon nanotubes fabricated by diamond wire drawing dies, Nano Lett. 8 (2008) 1071–1075, https://doi.org/10.1021/nl073007o.
[28] Z. Qiu, D. He, Y. Wang, X. Zhao, W. Zhao, H. Wu, High performance asymmetric supercapacitors with ultrahigh energy density based on hierarchical carbon nanotubes@NiO core-shell nanosheets and defect-introduced graphene sheets with hole structure, RSC Adv. 7 (2017) 77843, https://doi.org/10.1039/c6ra27369f.
[29] M.J. Chatterjee, A. Ghosh, A. Mondal, D. Banerjee, Polyaniline-single walled carbon nanotube composite-a photocatalyst to degrade rose bengal and methyl orange dyes under visible-light illumination, RSC Adv. 7 (2017) 36403, https://doi.org/10.1039/c7ra03855k.
[30] J.P. Pouget, M.E. Józefowicz, A.J. Epstein, X. Tang, A.G. MacDiarmid, X-ray structure of Polyaniline, Macromolecules 24 (1991) 779–789, https://doi.org/10.1021/ma00003a022.
[31] K. Datta, P. Ghosh, M. a More, M.D. Shirsat, a Mulchandani, Controlled functionalization of single-walled carbon nanotubes for enhanced ammonia sensing: a comparative study, J. Phys. D Appl. Phys. 45 (2012) 355305, , https://doi.org/10.1088/0022-3727/45/35/355305.
[32] V. Lordi, N. Yao, Molecular mechanics of binding in carbon-nanotube–polymer composites, J. Mater. Res. 15 (2000) 2770–2779, https://doi.org/10.1557/JMR.2000.0396.
[33] R. Chan Yu King, F. Roussel, J.F. Brun, C. Gors, Carbon nanotube-polyaniline nanohybrids: influence of the carbon nanotube characteristics on the morphological, spectroscopic, electrical and thermoelectric properties, Synth. Met. 162 (2012) 1348–1356, https://doi.org/10.1016/j.synthmet.2012.05.029.
[34] S. He, J. Wei, F. Guo, R. Xu, C. Li, X. Cui, H. Zhu, K. Wang, D. Wu, A large area, flexible polyaniline/buckypaper composite with a core–shell structure for efficient supercapacitors, J. Mater. Chem. A 2 (2014) 5898–5902, https://doi.org/10.1039/C4TA00089G.
[35] A.N. Papathanassiou, I. Sakellis, J. Grammatikakis, Universal frequency-dependent ac conductivity of conducting polymer networks, Appl. Phys. Lett. 91 (2007), https://doi.org/10.1063/1.2779255.
[36] G. Williams, D.C. Watts, Non-symmetrical dielectric relaxation behaviour arising from a simple empirical decay function, Trans. Faraday Soc. 66 (1970) 80, https://doi.org/10.1039/tf9706600080.
[37] M. El Hasnaoui, M.P.F. Graça, M.E. Achour, L.C. Costa, Electric modulus analysis of carbon black/copolymer composite materials, Mater. Sci. Appl. 2 (2011) 1421–1426, https://doi.org/10.4236/msa.2011.210192.
[38] V. Alzari, D. Nuvoli, V. Sanna, T. Caruso, S. Marino, N. Scaramuzza, Study of polymeric nanocomposites prepared by inserting graphene and / or Ag, Au and ZnO nanoparticles in a TEGDA polymer matrix, by means of the use of dielectric

spectroscopy, AIP Adv. 6 (2016) 035005, , https://doi.org/10.1063/1.4943672.
[39] R. Islam, A.N. Papathanassiou, R. Chan-Yu-King, F. Roussel, On the sign of the relaxation activation energy for interfacial polarization in reduced graphene oxide–based nano-composites, Appl. Phys. Lett. 109 (2016) 182901, , https://doi.org/10.1063/1.4966273.
[40] L.K.H. Van Beek, Dielectric behavior of heterogeneous systems, Prog. Dielectr. (1967) 71–114.
[41] D. Stauffer, A. Aharony, Introduction to percolation theory, Taylor Francis 1 (1991) 192, https://doi.org/10.1103/RevModPhys.63.991.
[42] C. Grimaldi, Theory of percolation and tunneling regimes in nanogranular metal films, Phys. Rev. B 89 (2014) 214201, , https://doi.org/10.1103/PhysRevB.89.214201.
[43] H. Namikawa, Characterization of the diffusion process in oxide glasses based on the correlation between electric conduction and dielectric relaxation, J. Non. Solids 18 (1975) 173–195, https://doi.org/10.1016/0022-3093(75)90019-8.
[44] A.N. Papathanassiou, J. Grammatikakis, I. Sakellis, S. Sakkopoulos, E. Vitoratos, E. Dalas, Hopping charge transport mechanisms in conducting polypyrrole: studying the thermal degradation of the dielectric relaxation, Appl. Phys. Lett. 87 (2005) 154107, , https://doi.org/10.1063/1.2103388.
[45] A.N. Papathanassiou, I. Sakellis, E. Vitoratos, S. Sakkopoulos, Interfacial and space charge dielectric effects in Polypyrrole/Zinc Oxide composites, Synth. Met. 228 (2017) 41–44, https://doi.org/10.1016/j.synthmet.2017.03.019.